

Disturbed Stress Field Model for Unreinforced Masonry

Luca Facconi, Ph.D.¹; Giovanni Plizzari²; and Frank Vecchio³

Abstract: The traditional smeared crack macromodels for the analysis of masonry structures consider masonry as a homogeneous material with the effects of mortar joints included in an average sense. This approach, suitable for the analysis of large structures, implicitly excludes the possibility of representing local elastic and inelastic mechanisms involving mortar joints. In this study, an innovative formulation based on the disturbed stress field model (DSFM) is proposed for the analysis of unreinforced masonry structures. The advancement introduced by the model lies in the possibility of simulating the global average behavior of the composite material in combination with the local nonlinear shear slip response of both bed and head joints. This paper describes the formulation of the model; as well, it presents results obtained from the simulation of tests performed on shear walls demonstrating the ability of the DSFM to reproduce the structural response of masonry structures. DOI: 10.1061/(ASCE)ST.1943-541X.0000906. © 2013 American Society of Civil Engineers.

Author keywords: Unreinforced masonry; Smeared crack; Joints shear slip; Shear walls; Finite-element analysis; Plane stress; Concrete and masonry structures.

Introduction

Masonry is a composite building material composed of units (e.g., stones, bricks, blocks) connected by mortar joints placed horizontally and vertically within the brickwork. The mortar joints normally act as planes of weakness because of their low tensile and shear bond strengths. The presence of the joints makes masonry an orthotropic material having directional properties that depend on the orientation of the joints relative to the applied principal stresses. As with reinforced concrete, three different approaches can be used in modeling the behavior of masonry elements: the discrete crack approach, the homogenization techniques, and the smeared crack approach.

The discrete crack approach is based on a micromodeling concept in which the units and mortar are modeled separately involving the consideration of the properties of each component.

Homogenization techniques represent another growing research field among the masonry community. The method allows determination of constitutive relations in terms of average stresses and strains starting from the constitutive properties of the single components; a complete review of the most important advances in this research field can be found in Lourenço et al. (2007). On the one hand, these techniques would avoid performing expensive tests and changing the material model when changes in single components properties occur; on the other hand, the bricks and mortar properties are often unknown and so they have to be determined by inverse fitting of the composite material properties.

The smeared crack approach follows a macromodeling concept in which the blended properties of the masonry material are taken into account. Attempts to develop macromodels for representing unreinforced masonry have been reported by Lourenço and Rots (1997) and Lotfi and Shing (1991), with the former especially proving to be a useful tool capable of providing reasonably accurate predictions of structural behavior in the case of small shear walls as well as large unreinforced masonry buildings. However, despite their simplicity and low computation cost, macromodels present some limitations that are a direct consequence of the assumptions on which they are based. The approach usually adopted involves modeling masonry with material laws that consider the properties and behavior of mortar joints and units in a blended or smeared sense.

This paper presents an alternative phenomenological macromodel for masonry that is based on the disturbed stress field model (DSFM) specifically developed by Vecchio (2000, 2001) for reinforced concrete. Unlike conventional smeared crack models, the DSFM for masonry is able to combine the average macroscopic representation of the material behavior with the local shear stress-shear slip response of mortar joints. In addition to the typical advantages of macromodels (low computational costs, synthetic representation of the structural behavior), the proposed formulation attempts to enable the prediction of structural response even in cases in which the damage mechanism is governed by the local behavior of masonry joints. A complete discussion of the model and its performance can be found in Facconi (2012).

The formulation of the DSFM reported in this paper can be used only for the analysis of masonry structures subjected to monotonic loading conditions. Future improvement of the proposed model will aim to develop procedures for simulating the cyclic response of masonry structures.

Overview of Conceptual Model

Depicted in Fig. 1, for the purposes of discussion, is a typical unreinforced masonry shear wall. Assuming that such a structural element is reasonably larger than the single masonry components, the joints and units can be considered smeared over the continuum area. Thus, a field of internal average stresses and strains sustaining

¹Postdoctoral Fellow, Dept. of Civil, Architectural, Environmental, Land Planning Engineering and Mathematics, Univ. of Brescia, Via Branze 43, 25123 Brescia, Italy (corresponding author). E-mail: luca.facconi@ing.unibs.it

²Professor, Dept. of Civil, Architectural, Environmental, Land Planning Engineering and Mathematics, Univ. of Brescia, Via Branze 43, 25123, Brescia, Italy.

³Professor, Dept. of Civil Engineering, Univ. of Toronto, 35 St. George St., Toronto, ON, Canada M5S 1A4.

Note. This manuscript was submitted on January 14, 2012; approved on July 2, 2013; published online on July 4, 2013. Discussion period open until April 27, 2014; separate discussions must be submitted for individual papers. This paper is part of the *Journal of Structural Engineering*, © ASCE, ISSN 0733-9445/04013085(11)/\$25.00.

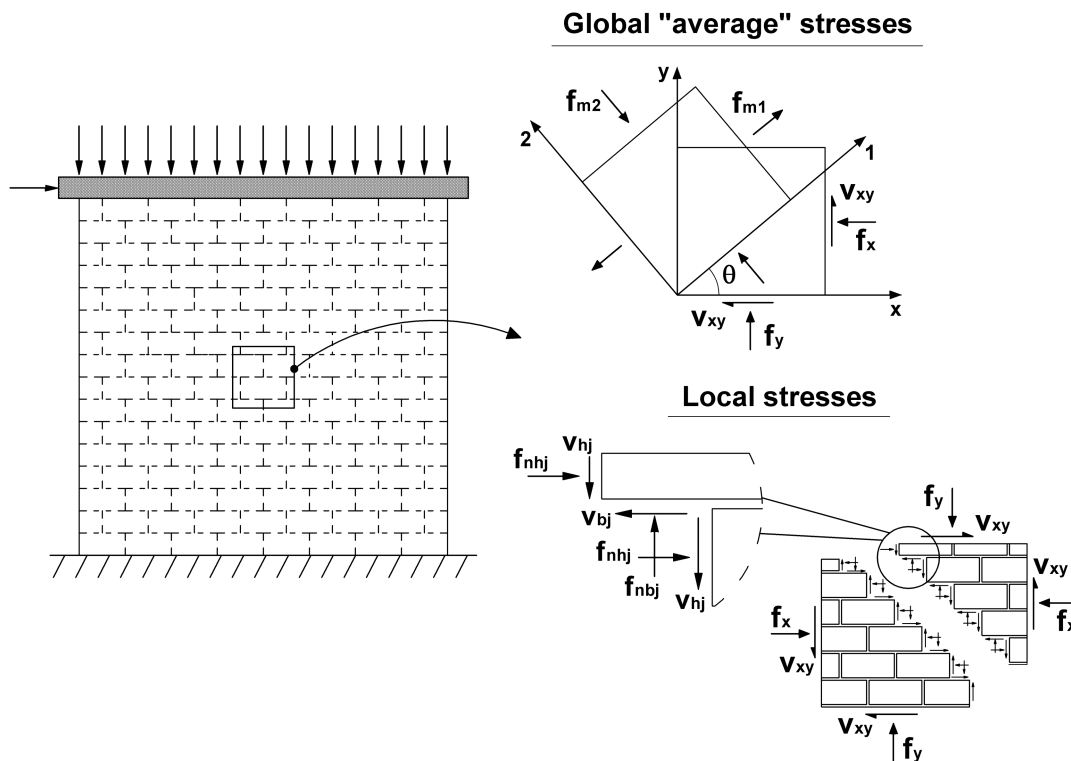


Fig. 1. Disturbed stress field approach for masonry elements

the load applied to the structure may be defined. With masonry, both compressive and tensile stresses are active components of the internal load-resisting mechanism. Consider a small region of the wall that is large enough to span a number of joints and units but, at the same time, is sufficiently contained such that the sectional forces can be considered uniform. Within that area, the material is subjected to a field of average principal tensile and compressive stresses (f_{m1} , f_{m2}) that are related to the corresponding average strains by appropriate nonlinear constitutive relationships that characterize the behavior of the composite. As a consequence of the principal tensile stresses, the composite material can experience smeared cracks oriented in the principal average compressive stress direction. The orthotropic behavior of masonry is mainly due to the presence of thin mortar joints that act as planes of weakness. To provide equilibrium to the masonry membrane element subjected to principal average stresses, a set of local shear (v_{bj} , v_{hj}) and normal (f_{nbj} , f_{nhj}) stresses develop along bed and head joints. The local shear stress acting parallel to the joint gives rise to shear rigid body slip between the two unit-mortar interfaces that delimit the joint. This local deformation has to be combined with the average (smeared) strains to obtain the total strains that represent the deformation of the whole masonry membrane. Finally, the internal load-resisting mechanism may be considered as consisting of a field of average stresses locally disturbed by stresses acting along the mortar thin joints.

The formulation of the DSFM presented in this paper aims to pursue the previously mentioned conceptual description of the masonry behavior by appropriate equilibrium, compatibility, and constitutive relationships.

Equilibrium Conditions

Fig. 2(a) shows the free body diagram of a masonry element subjected to uniform stresses, $[f] = \{f_x, f_y, v_{xy}\}$, applied along

the membrane edges. The masonry element consists of several units connected by mortar joints that are arbitrarily inclined at an angle α with respect to the element reference axes $x - y$; the local reference axes $x' - y'$ are, respectively, parallel and perpendicular to the bed joints. As is typically the case in practice, the head and bed joints are considered perpendicular to each other. The forces applied to the masonry element are resisted by internal stresses acting in the masonry components. That said, the equilibrium of the membrane element has to be evaluated globally in terms of average smeared stresses and locally by considering the stresses acting along the mortar joints.

In the model, masonry is considered as an orthotropic material that may experience the formation of smeared cracks; thus, the average principal masonry stresses f_{m2} and f_{m1} [Figs. 3(b and c)] act parallel and perpendicular to the crack plane whose direction is defined by the angle θ . In order to take into account the tension-softening behavior of masonry, the principal stress f_{m1} is

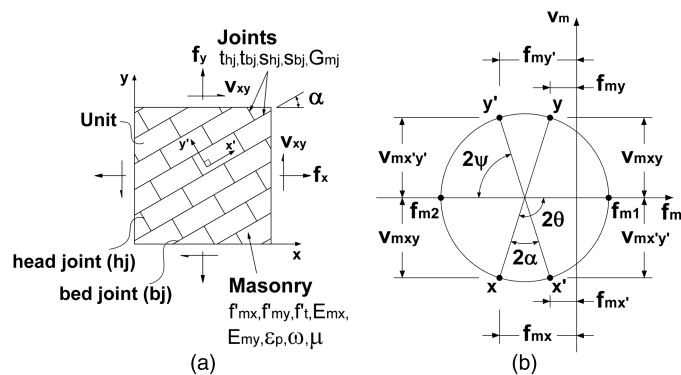


Fig. 2. Unreinforced masonry element: (a) geometry and loading condition; (b) Mohr's circle for average stresses in masonry

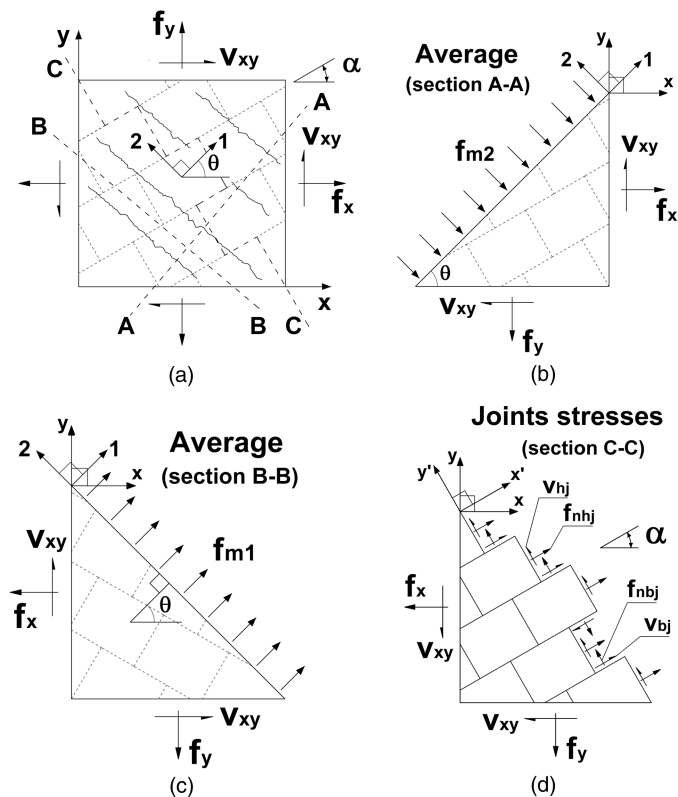


Fig. 3. Equilibrium conditions of unreinforced masonry element: (a) applied stresses; (b) perpendicular to crack plane; (c) parallel to crack plane; (d) at joints location

considered active even after cracking. To relate the average net strains to the global stresses applied to the element, the following relationship may be used:

$$[f] = \{f_x, f_y, v_{xy}\} = [D_m][\varepsilon_m] \quad (1)$$

where $[D_m]$ = material secant stiffness matrix for masonry; $[f]$ = stress vector referred to by the global reference system $x-y$; and $[\varepsilon_m]$ = net strain acting in the masonry. Once the principal stresses are determined, the internal masonry stresses f_{mx} , f_{my} , and v_{mxy} can be simply evaluated by means of the Mohr's circle of stress reported in Fig. 2(b).

Along the crack planes, perpendicular to the principal tensile stress direction [Fig. 3(a)], no shear stresses are considered acting. The local internal stresses acting at the joint locations may be derived from the equilibrium conditions of the unreinforced masonry element; therefore, with reference to the Mohr's circle of stress shown in Fig. 2(b) and to the equilibrium conditions depicted in Fig. 3(d), the joints stresses result from standard relations

$$f_{mx'} = f_{nhj} = [(f_{m1} + f_{m2}) + (f_{m1} - f_{m2}) \cdot \cos 2\psi]/2 \quad \text{and} \\ f_{my'} = f_{nbj} = [(f_{m1} + f_{m2}) - (f_{m1} - f_{m2}) \cdot \cos 2\psi]/2 \quad (2)$$

$$v_{mx'y'} = v_{bj} = v_{hj} = [(f_{m1} - f_{m2}) \cdot \sin 2\psi]/2 \quad (3)$$

where $\psi = \theta - \alpha$ is the difference between the angle θ normal to the crack direction and the angle α , which defines the direction of the bed joints. According to the equilibrium condition represented by Eq. (2), the head joints shown in Fig. 3(d) are assumed to be all aligned and not staggered as is typically the case in brick masonry;

future developments will be addressed to improve this simplifying assumption.

Compatibility Relations

The compatibility conditions that characterize the response of the masonry elements are represented by the illustrations shown in Fig. 4. It is assumed that total deformations exhibited by the masonry element turn out from the superposition of two components: the former is the strain resulting from the deformation of the continuum due to the applied stresses, with the cracks considered smeared within the element area; the latter is represented by the strain that results from the rigid body slip occurring along bed and head joints. With reference to an arbitrary $x-y$ reference system, it is the net strains $[\varepsilon_m] = \{\varepsilon_{mx}, \varepsilon_{my}, \gamma_{mxy}\}$ due to average constitutive response that must be employed within appropriate constitutive relationships to determine the average masonry stresses. Because the model in this paper is based on a principal strain approach, Mohr's circle of strain shown in Fig. 4(a) can be used to determine the principal strains from the net strains

$$\varepsilon_{m1}, \varepsilon_{m2} = \frac{\varepsilon_{mx} + \varepsilon_{my}}{2} \pm \frac{1}{2} [(\varepsilon_{mx} - \varepsilon_{my})^2 + \tau_{mxy}^2]^{1/2} \quad (4)$$

The inclination of the cracks within the continuum is assumed to be coincident with the inclination of the net principal strains, θ , and the inclination of the principal stresses, θ_σ . That is, the rotating crack concept is adopted, thus

$$\theta = \theta_\sigma = \frac{1}{2} \tan^{-1} [\gamma_{mxy} / (\varepsilon_{mx} - \varepsilon_{my})] \quad (5)$$

It is assumed that the masonry element consists of rectangular bricks that are mutually connected by head and bed mortar joints having a constant thickness (t_{hj} , t_{bj}) and spacing (s_{hj} , s_{bj}) [Fig. 4(b)]. The shear stress acting parallel to the joint causes a local slip displacement along the joint plane whose magnitude is δ_{bj}^s for the bed joints and δ_{hj}^s for the head joints. Thus, the average shear strain due to the slip of bed and head joints may be respectively defined as follows:

$$\gamma_{bj}^s = \delta_{bj}^s / s_{bj}; \quad \gamma_{hj}^s = \delta_{hj}^s / s_{hj} \quad (6)$$

The total slip strain can be decomposed into orthogonal components relative to the $x-y$ reference system, which can be computed respectively for bed $[\varepsilon_{bj}^s]$ and head $[\varepsilon_{hj}^s]$ joints by Mohr's circle construction [Fig. 4(b)]

$$[\varepsilon_{bj}^s] = \{\varepsilon_{x,bj}^s, \varepsilon_{y,bj}^s, \gamma_{xy,bj}^s\} = \{\gamma_{bj}^s/2 \cdot \sin(2\alpha), \\ -\gamma_{bj}^s/2 \cdot \sin(2\alpha), -\gamma_{bj}^s \cdot \cos(2\alpha)\} \quad (7)$$

$$[\varepsilon_{hj}^s] = \{\varepsilon_{x,hj}^s, \varepsilon_{y,hj}^s, \gamma_{xy,hj}^s\} = \{-\gamma_{hj}^s/2 \cdot \sin(2\alpha), \gamma_{hj}^s/2 \\ \cdot \sin(2\alpha), \gamma_{hj}^s \cdot \cos(2\alpha)\} \quad (8)$$

The sum of the resultant vectors provides the equivalent average strain slip vector $[\varepsilon^s]$

$$[\varepsilon^s] = [\varepsilon_{bj}^s] + [\varepsilon_{hj}^s] \quad (9)$$

In addition to the net and slip strains, the masonry element may experience two other types of strain offset effects (Vecchio 1992, 2000): elastic strain offsets $[\varepsilon_m^0]$ arising from mechanisms such as thermal expansion or mechanical expansion, and plastic

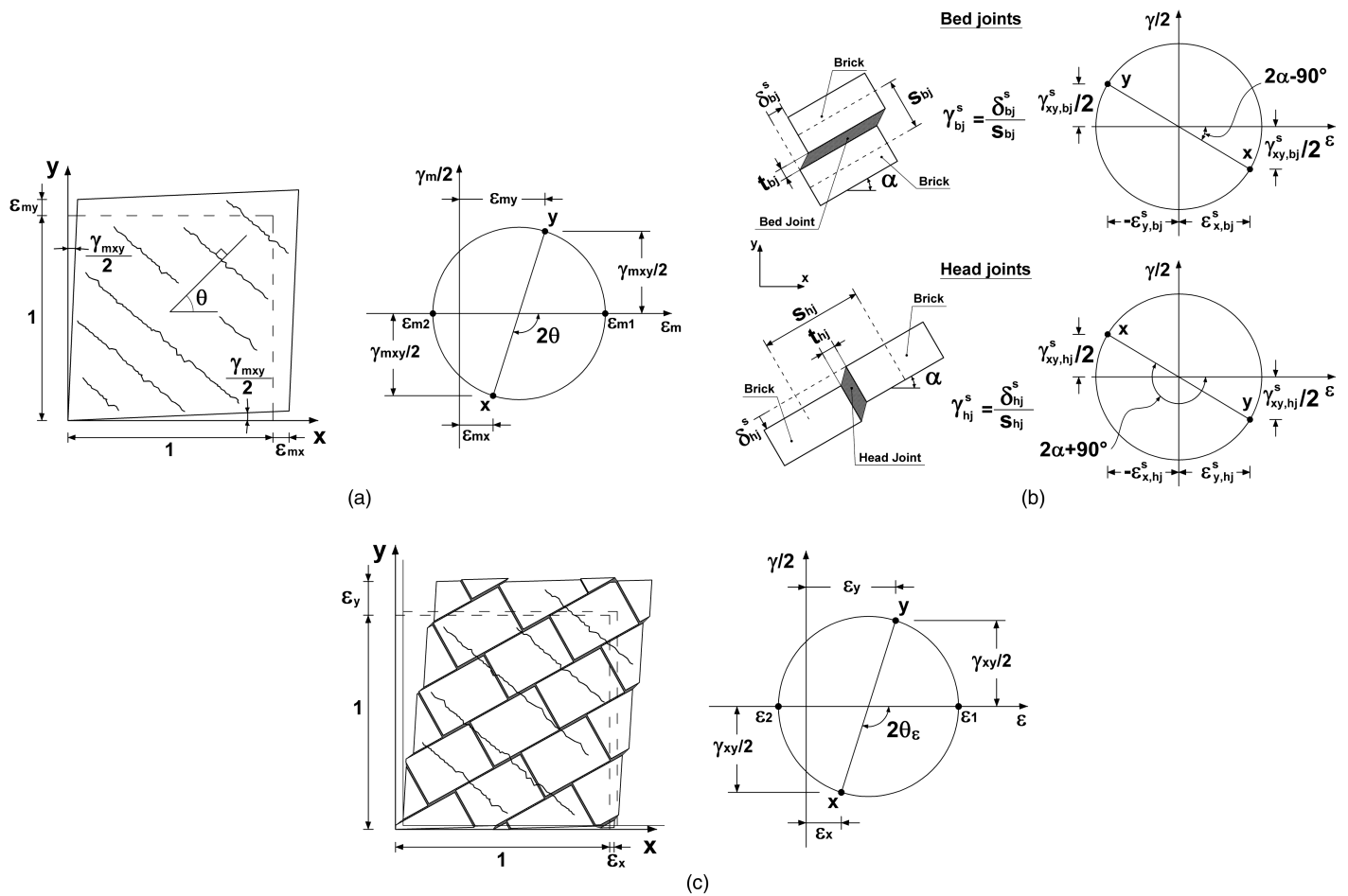


Fig. 4. Compatibility conditions: (a) average (smeared) strains for masonry; (b) deformations due to local rigid body slip along the joints; (c) total (combined) deformation of masonry material

strain offsets $[\varepsilon_m^p]$, which may arise from cyclic loading conditions or loading into postpeak levels. By considering such effects [Fig. 4(c)], the total (apparent) strain $[\varepsilon] = (\varepsilon_x, \varepsilon_y, \gamma_{xy})$ relative to the global reference system results from the following relationship:

$$[\varepsilon] = [\varepsilon_m] + [\varepsilon^s] + [\varepsilon_m^o] + [\varepsilon_m^p] \quad (10)$$

The angle θ_ε , which denotes the inclination of the total principal strains, can be derived as follows:

$$\theta_\varepsilon = \frac{1}{2} \cdot \tan^{-1}[\gamma_{xy}/(\varepsilon_x - \varepsilon_y)] \quad (11)$$

The cracks, smeared over the area of the masonry element, are characterized by an average width w and average spacing s . In most old and modern masonry structures, units are generally much stiffer and stronger than mortar and joints have a smaller thickness compared with single units; therefore, it is reasonable to assume that in a masonry element cracks tend generally to form into the joints before bricks. In view of this, one can define nominal crack spacings in the x' - and y' -directions, denoted $s_{x'}$ and $s_{y'}$, which correspond to the head joints spacing s_{hj} and the bed joints spacing s_{bj} , respectively. Hence, by taking into account the direction α of bed joints also considered in Eqs. (7) and (8), the average crack spacing in the cracked continuum may be calculated as

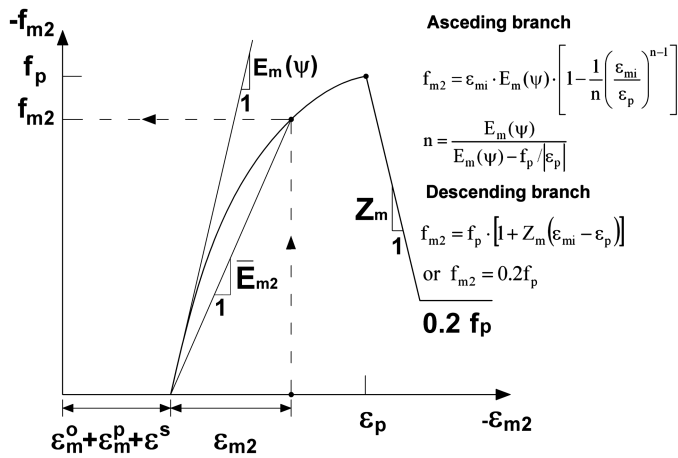
$$s = \left(\frac{\sin \psi}{s_{hj}} + \frac{\cos \psi}{s_{bj}} \right)^{-1} \quad (12)$$

The average tensile net stain and the average crack spacing can be used to estimate the average crack width w through the following simple relationship:

$$w = \varepsilon_{m1} \cdot s \quad (13)$$

Masonry Compressive Stress-Strain Modeling

Compression stress-strain relationships for masonry are similar to those for concrete and may be represented by similar equations (Pauley and Priestley 1992). The compressive prepeak behavior of masonry is reasonably defined when the initial tangent elastic modulus (E_m), the average compressive strength (f'_m), and the strain at peak ε_0 are known. In many of the stress-strain models typically used to represent the response of concrete in compression [e.g., Kent and Park (1971), Fujii et al. (1988)], the ascending branch is described by a parabolic function that usually represents sufficiently well the actual response of the material. Though a parabolic representation of the prepeak compressive stress-strain curve is also considered suitable for masonry, in this paper the alternative formulation proposed by Hoshikuma et al. (1997) for confined reinforced concrete is used (Fig. 5). Unlike other models, the Hoshikuma formula is based on a function that considers the initial elastic modulus of masonry independently of the



compressive strength and the strain at peak. This approach, implemented in the DSFM, was found to be more effective in modeling the compression response of masonry structures. The falling branch of the stress-strain relationship is provided by the modified Kent-Park model proposed by Priestley and Elder (1983) for masonry. This model consists of a linear descending branch and a final horizontal plateau at 20% of the masonry compressive strength. The slope Z_m of the linear descending branch is given by

$$Z_m = [(3 + 0.29 \cdot f_j) / (145 \cdot f_j - 1,000) - 0.002]^{-1} \leq 1 \quad (14)$$

where f_j = mortar compressive strength. The falling branch doesn't start from a peak strain value of 0.0015, as was assumed in the original formulation, but from the peak strain ϵ_p determined by Eq. (19). The resultant stress-strain curve represented in Fig. 5 is shifted along the horizontal axis to include the effect of plastic and elastic strain offsets.

As with concrete, cracked masonry may exhibit a compression softening effect due to tensile strain acting in the transverse direction (Lotfi and Shing 1991), which can significantly reduce the compressive strength of the composite. In this paper, the compression softening effect is captured by a softening parameter β_d applied to the uniaxial compressive strength, ranging from 0 to 1, whose value is found from the following formula:

$$\beta_d = (1 + C_s \cdot C_d)^{-1} \leq 1 \quad (15)$$

in which the factors C_d and C_s are calculated according to the Vecchio 1992-A model (Vecchio and Collins 1993)

$$C_d = \begin{cases} 0 & \text{if } r < 0.28 \\ 0.35 \cdot (r - 0.28)^{0.8} & \text{if } r \geq 0.28 \end{cases}; \quad C_s = 0.55 \quad (16)$$

where $r = \epsilon_{m1} / \epsilon_{m2}$.

Masonry exhibits different directional properties due to the mortar joints acting as planes of weakness. Hence, the material failure cannot be simply defined in terms of principal stresses but needs an additional parameter, i.e., the bed joint orientation relative to the principal stresses direction. Ganz (1985) proposed an analytical failure criterion for masonry subjected to in-plane forces. Ganz's formulation starts with the assumption that a complete failure criterion for masonry materials has to take into account the possible failure of the components (bricks, mortar joints) as well as the failure of the composite material. Bricks are considered as prismatic blocks having internal vertical perforations perpendicular to the bed joints; thus, each unit is decoupled into

an uniaxial and a biaxial stressed component having perfect rigid-plastic behavior. Mortar joints are subjected to stresses acting parallel and perpendicularly to the joint plane. Shear failure of mortar bed joints is governed by means of a modified Coulomb's yield criterion in which the failure in compression of the mortar is excluded because of the triaxial compressive state of stress acting in the joints. Moreover, recognizing the usual weakness of the head joints due to the partial or total lack of mortar, the shear strength of head joints is neglected. The complete failure criterion for masonry with tensile strength is obtained from the linear combination of different failure surfaces derived from the equilibrium of the materials components (Ganz 1985). The original formulation of such a criterion was expressed in terms of global stresses and cannot be directly employed in a model based on a principal stress concept such as the DSFM. By reformulating the equations of Ganz's yield criterion in terms of principal stresses and restricting the failure domain to the biaxial compressive state of stress, a failure surface similar to the one reported in Fig. 6 is obtained. To completely define such a surface, some basic masonry parameters have to be known, i.e., the average compressive strength evaluated in the x' -axis direction ($f_{mx'}$), the average compressive strength evaluated in the y' -axis direction ($f_{my'}$), the friction angle (φ) and the cohesion (c) of mortar bed joints, the ratio between the tensile strength and the compressive strength in the x -direction (ω_m), and the value of the unit-mortar interface tensile strength (f_t'). As typical in the practice, bed joints are horizontal ($\alpha = 0$) so one may assume $f_{mx} = f_{mx'}$ and $f_{my} = f_{my'} = f_m'$ (f_m' = peak strength measured in the direction perpendicular to bed joints). The failure surface represented in Fig. 6 is a function of both the principal stresses (f_1, f_2) and the angle θ , which defines the orientation of the principal stresses relative to bed joints. As is clearly shown in Fig. 6, the masonry compressive strength f_2 depends on the value of the transverse compressive stress f_1 ; in fact, by increasing the ratio f_1/f_2 , the resultant failure curve shifts upward and the maximum compressive strength of the composite material is increased as well. Dividing the maximum masonry strength $f_2(f_1, \theta)$ obtained from the failure criterion by the masonry strength f_{my} , one obtains the reduction factor β_m

$$\beta_m = \frac{f_2(f_1, \theta)}{f_{my}} \leq 1 \quad (17)$$

Hence, with the determination of the reduction factors β_d and β_m , the peak stress f_p and the strain at peak stress ϵ_p are evaluated as follows:

$$f_p = -\beta_d \cdot \beta_m \cdot f_m' \quad (18)$$

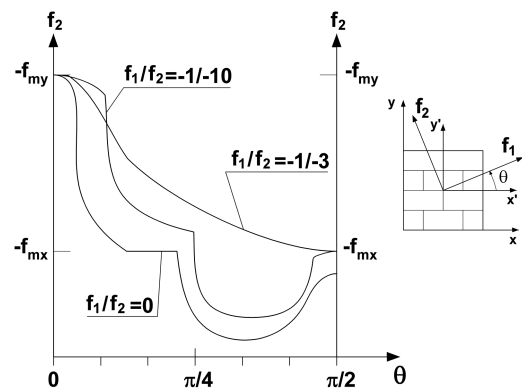


Fig. 6. Ganz's failure criteria for masonry in compression: principal stresses formulation

$$\varepsilon_p = -\beta_d \cdot \varepsilon_0 \quad (19)$$

where $f'_m = f_{my}$; and ε_0 = compressive strain at peak stress f'_m . The reduction coefficient β_m is considered both in the uncracked and in the cracked stage of the material response.

The anisotropic behavior of masonry also affects the value of the initial elastic modulus E_m , with it being maximum in the direction perpendicular to the bed joints (E_{my}) and minimum in the direction parallel to the bed joints (E_{mx}). To provide a smooth transition from the maximum to the minimum value (i.e., a relationship that allows for the evaluation of E_m as a function of the angle ψ), the traditional elastic theory for orthotropic materials may be used. The proposed formulation is presented in the appendix.

Masonry Tensile Stress-Strain Modeling

Similarly to compression, masonry in tension is characterized by an orthotropic behavior both in the elastic and in the inelastic stage. In the elastic stage, masonry is assumed to be linear elastic until the principal tensile stress f_{m1} reaches the maximum tensile strength f'_t and, as a consequence, the cracking process begins. Hence, before cracking, the following linear relation is used:

$$f_{m1} = E_m(\psi) \cdot \varepsilon_{m1}, \quad 0 < \varepsilon_{m1} < \varepsilon_{cr} \quad (20)$$

where $E_m(\psi)$ = elastic modulus evaluated according to the formulation reported in the appendix to account for the elastic orthotropic behavior of masonry; and ε_{cr} = first cracking strain. In this paper, as a rough approximation, the tensile strength of the composite material is assumed to be constant and equal to the tensile strength of the joint-unit interface; the effect of the principal stress f_{m2} on the average tensile strength of the composite is not considered in the model at the moment. In view of the reasonable results provided by the first numerical simulations of some full-scale masonry structures, such an assumption has been considered acceptable and able to well approximate the effective tensile behavior of masonry. However, further refinements will be implemented in the model in order to also include the orthotropic tensile strength properties of the material.

After the cracking process has begun, the tensile stress in masonry does not abruptly drop to zero but decreases gradually, exhibiting a so-called tension-softening response. According to Van Der Pluijm and Vermeltoort (1991), the tensile response of unreinforced masonry may be represented by an exponential function to indicate the relationship between the tensile stress and the crack opening. In this paper, the exponential decay curve suggested by Hordjik et al. (1987) is used

$$f_{m1} = f'_t \left\{ \left[1 + \left(3 \frac{\varepsilon_{m1}}{\varepsilon_{tu}} \right)^3 \right] e^{-6.93 \frac{\varepsilon_{m1}}{\varepsilon_{tu}}} - 0.027 \frac{\varepsilon_{m1}}{\varepsilon_{tu}} \right\}, \quad \varepsilon_{m1} > \varepsilon_{cr} \quad (21)$$

Based on the value of the Mode-I fracture energy G_f^I , the ultimate tensile strain ε_{tu} may be determined as follows:

$$\varepsilon_{tu} = 5.136 \cdot \frac{G_f^I}{f'_t L_r} \quad (22)$$

where L_r = characteristic length; and f'_t = average uniaxial tensile strength of the masonry composite. The resultant tensile stress-strain relationship, including the effect of elastic and plastic strain offsets, is shown in Fig. 7. Reasonable values of the tensile fracture energy can be chosen in the range 0.005 – 0.02 N/mm for tensile bond strength values varying from 0.3 to 0.9 MPa.

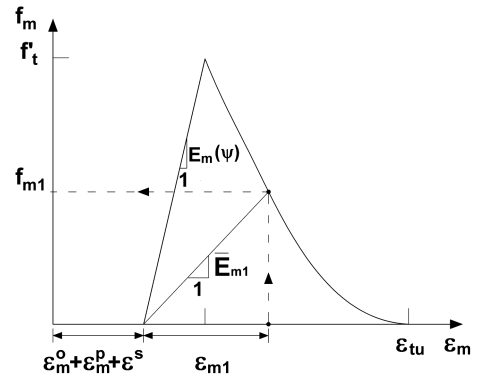


Fig. 7. Tensile stress-strain constitutive relation

Shear Slip Model for Masonry Joints

The shear behavior of mortar joints has been studied by many researchers; a comprehensive dissertation and literature review of the most prominent studies can be found in Guo (1991). Atkinson et al. (1989), for one, conducted servo-controlled direct shear tests to assess the response of brick masonry bed joints under monotonic and cyclic loading conditions. According to the results of these tests, the prepeak component of the shear-slip response curve can be represented by a hyperbolic equation in which the shear stiffness is not constant but is a function of both shear displacement and normal stress. Despite this, Rots (1997) showed that the prepeak shear-slip response may be reasonably assumed as linear elastic with a constant shear stiffness. The postcracking shear response of the joints may be reasonably represented by an exponential softening relationship whose subtended area represents the Mode-II fracture energy.

In this paper, as a first attempt at modeling the shear-slip response of masonry joints in the context of the DSFM approach, an elastic-plastic shear stress-strain relationship is adopted (Fig. 8). The slope of the linear elastic branch coincides with the masonry shear stiffness G_{mj} , whose value can be estimated by the usual relationship taken from the theory of elasticity (Hendry 1998)

$$G_{mj} = E_{my} / [2 \cdot (1 + \nu_{xy})] \quad (23)$$

where ν_{xy} = Poisson's coefficient of the composite material. The Young's modulus used to derive the value of G_{mj} is kept constant and equal to E_{my} . To determine the level ($v_{j,max}$) of the horizontal plastic plateau, a hyperbolic Mohr-Coulomb type yield criterion is used (Fig. 9). Similar to the yield criterion proposed by Lotfi and Shing (1994), it consists of a three-parameter hyperbola that

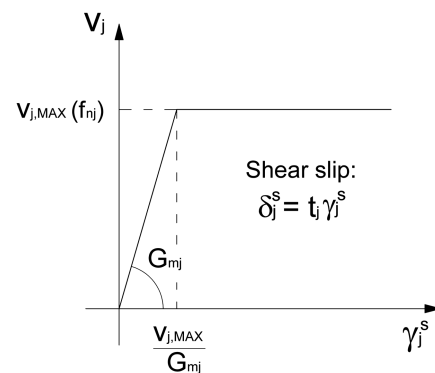


Fig. 8. Shear stress-strain relationship for bed and head joints

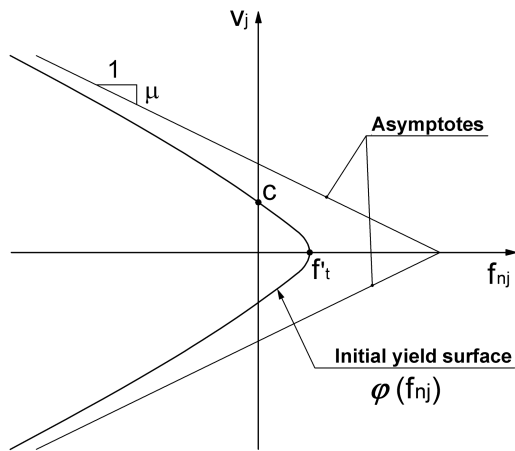


Fig. 9. Hyperbolic yield criterion

$$[D_m]' = \begin{bmatrix} \bar{E}_{m1} & 0 & 0 \\ 0 & \bar{E}_{m2} & 0 \\ 0 & 0 & \bar{G}_m \end{bmatrix} \quad (28)$$

where \bar{E}_{m1} , \bar{E}_{m2} , and \bar{G}_m = secant moduli. Once the net strains $[\varepsilon_m]$ resulting from Eq. (10) have been defined, the secant moduli turn out from the following relations (Vecchio 1992):

$$\bar{E}_{m1} = \frac{f_{m1}}{\varepsilon_{m1}}; \quad \bar{E}_{m2} = \frac{f_{m2}}{\varepsilon_{m2}}; \quad \bar{G}_m \cong \frac{\bar{E}_{m1} \cdot \bar{E}_{m2}}{\bar{E}_{m1} + \bar{E}_{m2}} \quad (29)$$

where f_{m1} and f_{m2} = principal stresses obtained from the correspondent principal stress-strain constitutive relationships (Figs. 5 and 7). The material stiffnesses matrix $[D_m]$ referred to the global reference system x - y results from the following transformation:

$$[D_m] = [T]^T [D_m]' [T] \quad (30)$$

where the transformation matrix $[T]$ is given by

$$[T] = \begin{bmatrix} \cos^2\psi & \sin^2\psi & \sin\psi \cos\psi \\ \sin^2\psi & \cos^2\psi & -\sin\psi \cos\psi \\ -2\sin\psi \cos\psi & 2\sin\psi \cos\psi & (\cos^2\psi - \sin^2\psi) \end{bmatrix} \quad (31)$$

The element stiffness matrix $[k_m]$ may be evaluated from standard procedures that are simply summarized as

$$[k_m] = \int [B]^T [D_m] [B] dV \quad (32)$$

where $[B]$ depends on the adopted element displacement functions. To determine the prestrain nodal forces of a two-dimensional element, strain offsets have to be taken into account; with regard to the masonry joints shear-slip strain $[\varepsilon_s]$, the free nodal displacements $[r_m^s]$ are determined from the element geometry (Vecchio 1990), i.e.,

$$[r_m^s] = \int [\varepsilon^s] dA \quad (33)$$

Hence, from the free displacements the prestrain pseudonodal forces can be found as follows:

$$[F_m^*] = [k_m] [r_m^s] \quad (34)$$

Prestrain forces can be similarly defined for the elastic and plastic offset strains. The prestrain forces are added to the externally applied nodal loads $[F]$ to obtain the total force vector $[F^*]$. A routine procedure is then used to calculate the nodal displacement and the correspondent element strains $[\varepsilon]$. The latter allow finding the element stresses by the following relation:

$$[f] = [D_m] [\varepsilon] - [f^0] = [D_m] ([\varepsilon] - [\varepsilon^s]) \quad (35)$$

where $[f^0]$ = element pseudostress. In order to perform a nonlinear analysis of unreinforced masonry bidimensional elements, the previous formulations are included into a total load, iterative secant stiffness procedure (Fig. 10), which leads to a progressive refinement of the stiffness matrices $[D_m]$ as well as the element stiffness matrices $[k_m]$. To estimate the joint shear slip, a simple linear elastic procedure (Fig. 11) has been implemented at the sixth step of the iterative routine shown in Fig. 10. Through each iteration h , the joint shear stress v_j is calculated and the value of the joint shear slip δ_j^s is progressively estimated; if the joint is in the linear elastic stage [Eq. (25)], the value of the joint slip is given by Eq. (26) by considering the elastic shear modulus G_{mj} provided by Eq. (23); on the other hand, in case of joint yielding [Eq. (27)], the joint slip δ_j^s is

provides a smooth transition between the Mohr-Coulomb friction law and the tension cutoff yield criterion. The criterion can be expressed as follows:

$$F(f_{nj}, f'_t) = v_j^2 - \mu^2 (f_{nj} - f'_t)^2 + 2\rho (f_{nj} - f'_t) = 0 \quad (24)$$

where $\rho = [c^2 - (\mu f'_t)^2] / 2f'_t$ = radius of curvature of the yield curve at the vertex of the hyperbola; c = cohesion; and μ = slope of the hyperbola asymptotes (i.e., $\tan \varphi$). According to the proposed approach, the strength f'_t is assumed constant and equal to the maximum tensile strength of the mortar joint-brick interface. The slope of the hyperbola asymptote and the cohesion are kept constant and equal to their initial values both in the elastic and during the tension-softening stage. Moreover, dilatancy phenomena are not considered in the model and, as a consequence, joints cannot be subjected to normal displacement under shear stresses acting along the joint plane. Once the stress normal to head or bed joints f_{nj} is known, the maximum value of the joint shear stress $v_{j,\max}(f_{nj})$ is determined from the yield criterion. Therefore, if the following relationship is satisfied:

$$|v_j| \leq |v_{j,\max}(f_{nj})| \quad (25)$$

and the joint has not already experienced yielding in previous loading steps, then the shear slip is controlled by the linear elastic branch of the shear stress-strain relationship (Fig. 8) as follows:

$$\delta_j^s = |v_j| \cdot t_j / G_{mj} \quad (26)$$

where t_j = thickness of the joint. As soon as the yield condition is reached according to

$$|v_j| > |v_{j,\max}(f_{nj})| \quad (27)$$

then a friction plastic slip will occur.

Finite-Element Implementation

To determine the stiffness matrix $[k]$ for a single element, a material stiffness matrix $[D_m]$ has to be constructed to relate the stress $[f]$ to the strain $[\varepsilon]$. In the proposed model, cracked masonry is assumed as an orthotropic material in which Poisson's effects can be reasonably neglected. Thus, the material stiffness matrix $[D_m]'$ referred to principal stress directions 1,2 is given by

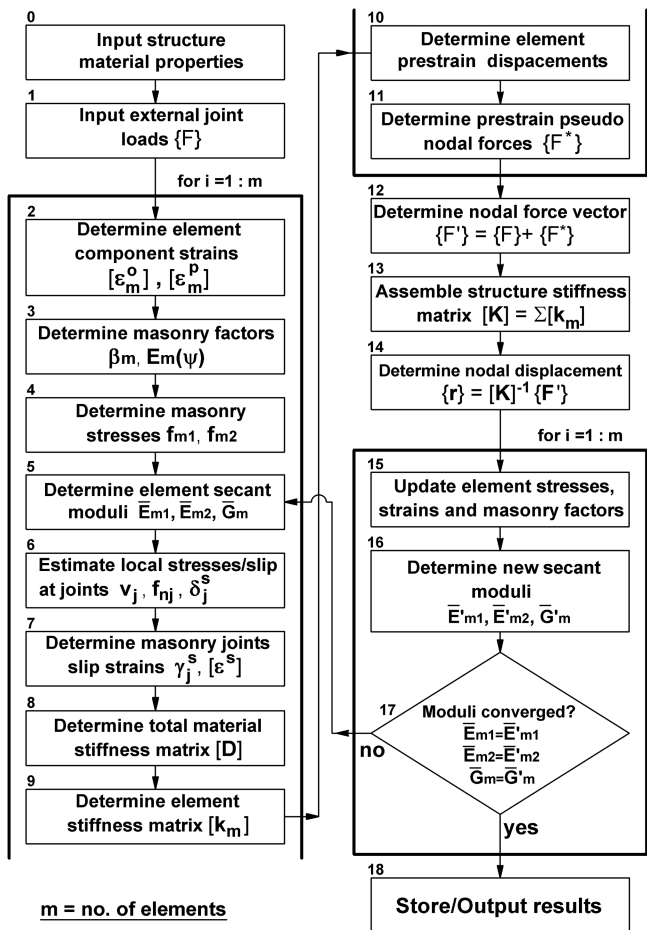


Fig. 10. Nonlinear analysis algorithm implemented in the finite-element program *VecTor 2*

found at each iteration by means of the secant shear modulus \bar{G}_{mj} obtained from the ratio of the current yielding stress value $v_{j,max}$ to the shear slip $\delta_j^{s(h-1)}$ resulting from the previous iteration $h-1$. The proposed iterative routine is entirely implemented in the finite-element program *VecTor 2* [Wong and Vecchio (2002)].

Model Validation

Verification studies of the proposed model for unreinforced masonry include comparisons with experimental tests performed by different researchers on a full-scale masonry wall and a building façade. Considering that the DSFM is based on a smeared crack approach, the results of the numerical analyses reported in the following naturally cannot completely reproduce local failure mechanisms involving individual units and masonry joints; however, it will be demonstrated that the DSFM is capable of capturing the global response of the structures and providing a qualitative representation of the crack pattern.

As a part of a comprehensive research program on the behavior of masonry shear walls, Ganz and Thürlimann (1984) carried out a series of tests on clay hollow brick walls subjected to shear and normal forces. The specimens (Fig. 12) were constructed of hollow clay bricks (300-mm long, 190-mm high, 150-mm wide) set on 10 different layers connected by 10-mm-thick cement mortar joints. One wall from the experiment, denoted as W1, was analyzed with the DSFM; such a specimen was subjected to initial uniform load of 415 kN ($p = 0.61$ MPa) applied over the entire length of the wall

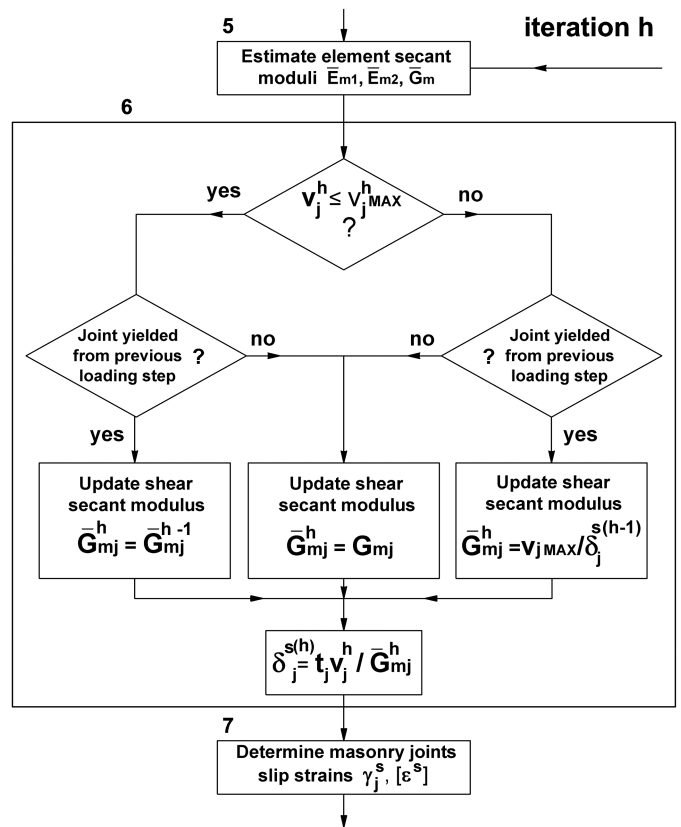


Fig. 11. Analysis procedure to determine joint shear slip

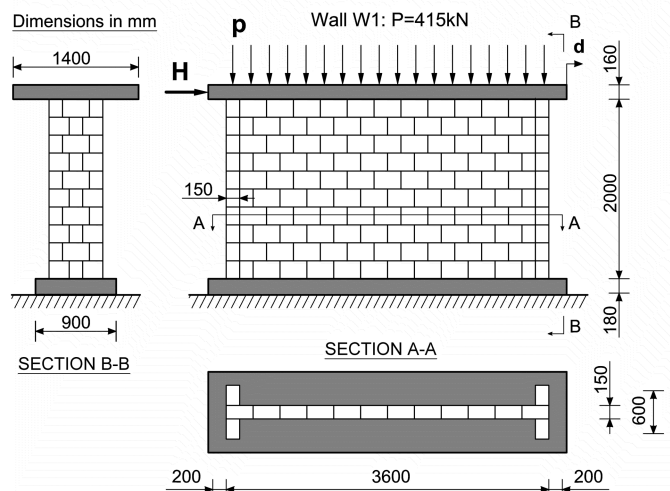


Fig. 12. Geometry of the ETH Zurich masonry shear walls

web and to an imposed displacement applied in a monotonic fashion at the top slab. The finite-element mesh used to simulate the walls consisted of 900 eight-degree-of-freedom (DOF) constant strain rectangular elements divided into two flange zones, a web zone, and two slab zones in order to distinguish the different thickness and material properties of the structure. The walls were assumed to be fully fixed at the base and the monotonic load was specified by applying a horizontal displacement to the top center node of the top slab. The values of the mechanical and geometrical parameters used in the numerical analysis to describe the masonry

Table 1. DSFM Parameters Used for Modeling ETH Zurich Walls Masonry Material

Materials and geometrical properties for DSFM	
f_{my} (MPa) ^a	= 7.61
f_{mx} (MPa) ^a	= 2.70
f_{ty} (MPa) ^a	= 0.03
ω_m (—) ^a	= 0.126
c (MPa) ^a	= 0.06
$\tan \varphi$ (—) ^a	= 0.81
μ (—) ^a	= 1.00
ν_{xy} (—) ^a	= 0.10
E_{my} (MPa) ^a	= 5,460
E_{mx} (MPa) ^a	= 2,463
G_f^I (N/mm)	= 0.02
ε_0 (mm/m)	= 2.0
t_{hj} (mm) ^a	= 10
t_{bj} (mm) ^a	= 10
s_{hj} (mm) ^a	= 300
s_{bj} (mm) ^a	= 190

^aParameters taken from Ganz and Thürlimann (1982, 1984).

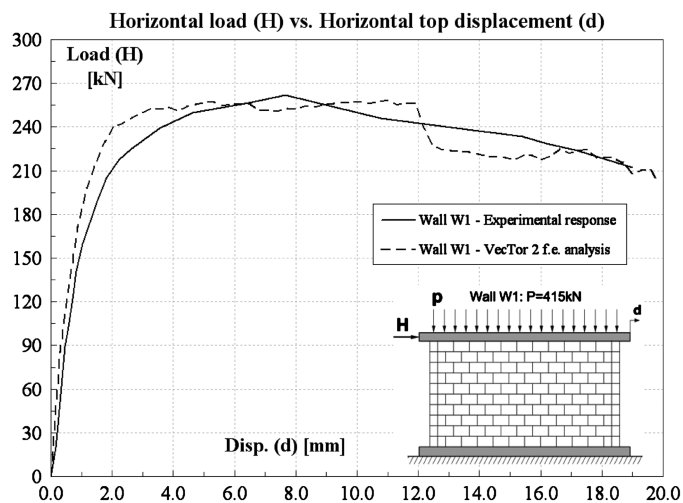
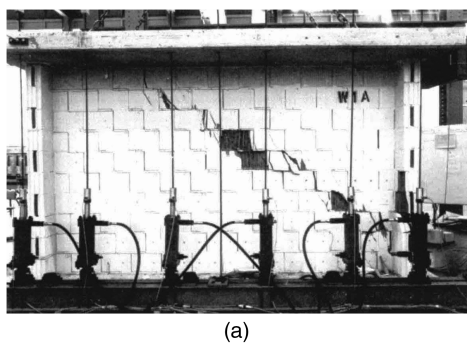


Fig. 13. Load-displacement response of the wall W1: experimental versus numerical response

behavior are summarized in Table 1; almost all the parameters coincide or are inferred from the masonry characteristics reported by Ganz and Thürlimann (1982, 1984) except for G_f^I and ε_0 , which were derived by fitting experimental data. The value of the compressive strength of mortar f_j , used in the postpeak Park-Kent



(a)

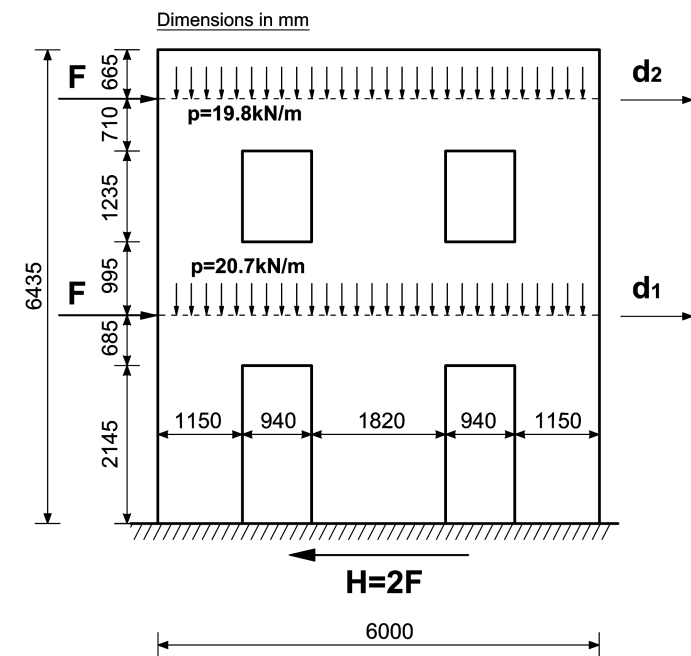
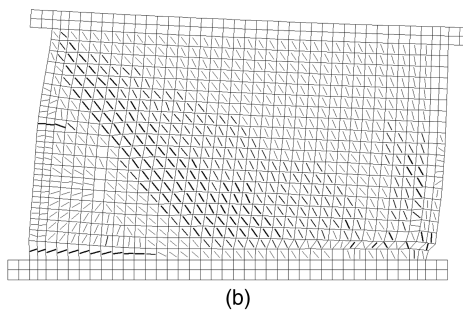


Fig. 15. Geometry of the masonry façade (Wall D) tested by Magenes et al. (1995)

model, was assumed to be equal to 23.9 MPa. The numerical and the experimental load-displacement response of wall W1 are compared in Fig. 13. From the figure it is apparent that the wall strength and stiffness are quite well predicted by the finite-element simulation. Moreover, the overall ductile behavior of the member, which is largely attributable to the combined effects of the initial vertical load and the lateral flanges, is also well captured by the model. As observed during the experimental test, the ultimate failure is mainly due to the progressive crushing of the lower corner of the wall in combination with the shear sliding mechanism involving the joints placed along the diagonal; as proven by Fig. 14, the simulation results reasonably agree with this experimental evidence.

The façade reported in Fig. 15, named Wall D, is a part of a full-scale two-story prototype tested under cyclic loading conditions by Magenes et al. (1995). The two-wythe solid brick wall was 6-m long, 6.44-m high, 250-mm thick, and had four openings. The floors consisted of a series of isolated steel beams that were used to apply both the horizontal and vertical loads during the test. The masonry weight per unit volume was 17 kN/m³, while the total vertical loads acting in correspondence to the first and the second floor were, respectively, 124 and 118 kN. The façade specimen was



(b)

Fig. 14. Wall W1 crack pattern: (a) experimental response at failure [Ganz and Thürlimann (1984), with permission from the Institute of Structural Engineering, ETH Zurich]; (b) numerical crack pattern and deformed mesh at a displacement $d = 19$ mm

Table 2. DSFM Parameters Used for Modeling Magenes et al.'s Façade Prototype

Materials and geometrical properties for DSFM	
f_{my} (MPa) ^a	= 6.20
f_{mx} (MPa) ^b	= 3.10
f_{ty} (MPa) ^b	= 0.18
ω_m (—)	= 0.045
c (MPa) ^a	= 0.23
$\tan \varphi$ (—) ^a	= 0.57
μ (—)	= 1.0
ν_{xy} (—) ^b	= 0.10
E_{my} (MPa) ^a	= 1,450
E_{mx} (MPa) ^b	= 1,000
G_f^l (N/mm) ^b	= 0.10
ε_0 (mm/m)	= 3.0
t_{hj} (mm) ^a	= 10
t_{bj} (mm) ^a	= 10
s_{hj} (mm) ^a	= 120
s_{bj} (mm) ^a	= 55

^aParameters taken from Magenes et al. (1995).

^bParameters taken from Berto et al. (2002).

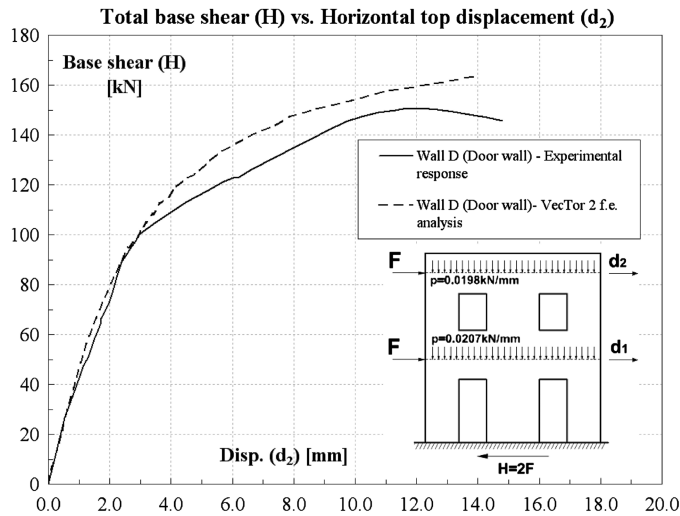


Fig. 16. Load-displacement response of Wall D: experimental versus numerical response

analyzed by using a finite-element model comprising 972 eight-DOF rectangular elements whose mechanical properties (Table 2) were estimated or derived from the literature (Magenes et al. 1995; Berto et al. 2002). Mortar strength f_j was assumed equal to 2 MPa (Magenes et al. 1995). Two equal shear forces were applied monotonically at floors level (Fig. 15) as imposed loads. The curves plotted in Fig. 16 represent, respectively, the experimental (hysteretic curves envelope) and numerical base shear (H) second floor displacement (d_2) response of Wall D. Relative to the experimental response, the analysis response correlates well in terms of maximum structure capacity; in fact, the predicted maximum base shear load ($H_{peak} = 168$ kN) and the correspondent displacement ($d_{peak} = 14.3$ mm) are, respectively, 12 and 16% higher than the experimental ones. The overall stiffness and ductility of the wall are quite well predicted by the model. The comparison of the numerical crack pattern detected at peak load [Fig. 17(b)] with the experimental failure pattern [Fig. 17(a)] shows the ability of the proposed model to predict the failure mechanisms. The progression of cracking observed during the finite-element simulation seems to reflect the experimental damaging process; indeed, cracking was initially limited to the spandrels between the openings until, at a lateral displacement $d_2 = 3.4$ mm, a diagonal shear crack appeared in the central pier at the ground floor. At the peak load both the central and the external right spandrel presented a shear failure mechanism in combination with flexural cracks located along the base of all the three ground floor piers. The piers at the second floor remained undamaged as observed during the experimental test.

Conclusions

An alternative formulation is proposed for the nonlinear analysis of unreinforced masonry structures subjected to monotonic loads; it is based on the DSFM, a smeared rotating crack model originally formulated for reinforced concrete. With respect to other continuum models reported in the literature, the innovation introduced lies in the ability of the DSFM to combine average behavior of the composite material with the local shear-slip response of masonry joints. By modeling the joints behavior separately, the proposed model is able to capture the local shear response of the joints in both the elastic and inelastic stages. Equilibrium, compatibility, and stress-strain relationships are formulated in terms of average

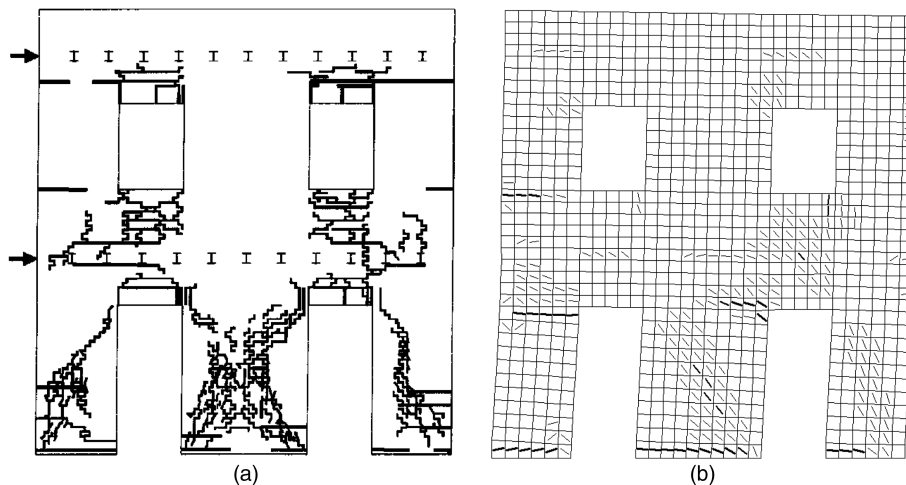


Fig. 17. Wall D crack pattern: (a) experimental response at failure (Magenes et al. 1995); (b) numerical crack pattern and deformed mesh at a displacement $d_2 = 14$ mm

principal stresses and strain. A modified version of Ganz's failure criterion is introduced to take into account the orthotropic compressive strength of the composite material. An elastic-plastic shear stress-slip relationship associated with a hyperbolic yield criterion is used to represent rigid body slip occurring along joints plane.

A verification of the proposed formulation was undertaken through comparisons with the results of two full-scale shear wall tests reported in the literature. The simulations provided reasonably accurate predictions of the walls' structural responses and demonstrated the ability of the model to represent well both ductile and brittle failure modes in masonry structures. Last, although the formulation is based on a smeared crack concept, the crack patterns observed in the test structures were captured quite well.

Further work is currently under way to improve the joints shear-slip model and to verify the effectiveness of the DSFM for the simulation of different types of unreinforced masonry structures.

Appendix. Evaluation of the Initial Tangent Modulus

With reference to the masonry element reported in Fig. 2(a), one can assume a global state of stress $[f]$ in which a uniaxial compressive stress is arbitrarily considered. To convert such a state of stress to the $x' - y'$ reference system, the following transformation can be used:

$$[f]' = [T]^{-T} \cdot [f]$$

where $[T]$ = transformation matrix [Eq. (31)]. For a linear elastic orthotropic material in a plane state of stress, the resultant strains are obtained from the following relationship:

$$[\varepsilon]' = \begin{bmatrix} \frac{1}{E_{mx}} & -\frac{\nu_{x'y'}}{E_{my}} & 0 \\ -\frac{\nu_{y'x'}}{E_{mx}} & \frac{1}{E_{my}} & 0 \\ 0 & 0 & \frac{1}{G_{x'y'}} \end{bmatrix} \cdot [f]'$$

where the shear modulus $G_{x'y'}$ is given by Weaver and Johnson (1984)

$$G_{x'y'} \approx \frac{E_{mx}E_{my}}{E_{mx}(1 + \nu_{x'y'}) + E_{my}(1 + \nu_{y'x'})} \quad \text{with} \quad \frac{\nu_{x'y'}}{\nu_{y'x'}} = \frac{E_{my}}{E_{mx}}$$

The strain vector $[\varepsilon]'$ can be transformed into global coordinates by the following transformation:

$$[\varepsilon] = [T]^T \cdot [\varepsilon]'$$

A reasonable estimate of the masonry initial tangent modulus $E_m(\psi)$ may be obtained by simply dividing the y component of the global stress $[f_y]$ by the correspondent global strain ε_y ; thus

$$E_m(\psi) = \frac{f_y}{\varepsilon_y}$$

References

Atkinson, R. H., Amadei, B. P., Saeb, S., and Sture, S. (1989). "Response of masonry bed joints in direct shear." *J. Struct. Eng.*, 10.1061/(ASCE)0733-9445(1989)115:9(2276), 2276–2296.

Berto, L., Sabetta, R., Scotta, R., and Vitaliani, R. (2002). "An orthotropic damage model for masonry structures." *Int. J. Numer. Methods Eng.*, 55(2), 127–157.

Facconi, L. (2012). "Fiber reinforced concrete and mortar for enhanced structural elements and repair of masonry walls." Ph.D. thesis, Dept. of Civil, Architectural, Environmental, Land Planning Engineering and Mathematics, Univ. of Brescia, Brescia, Italy.

Fujii, M., Kobayashi, K., Miyagawa, T., Inoue, S., and Matsumoto, T. (1988). "A study on the application of a stress-strain relation of confined concrete." *Proc. JCA Cement and Concrete*, Vol. 42, Japan Cement Association, Tokyo, 311–314.

Ganz, H. R. (1985). "Masonry walls subjected to normal and shear forces." Ph.D. thesis, Institute of Structural Engineering, ETH Zurich, Zurich, Switzerland (in German).

Ganz, H. R., and Thürlimann, B. (1982). "Tests on the biaxial strength of masonry." *Rep. No. 7502-3*, Institute of Structural Engineering, ETH Zurich, Zurich, Switzerland (in German).

Ganz, H. R., and Thürlimann, B. (1984). "Versuche an Mauerwerksscheiben unter Normalkraft und Querkraft." *Rep. No. 7502-4*, Institute of Structural Engineering, ETH Zurich, Zurich, Switzerland (in German).

Guo, P. (1991). "Investigation and modeling of the mechanical properties of masonry." Ph.D. thesis, McMaster Univ., Hamilton, Canada.

Hendry, A. W. (1998). *Structural masonry*, 2nd Ed., McMillan, London, U.K.

Hordjik, D. A., Reinhardt, H. W., and Cornelissen, H. A. W. (1987). "Fracture mechanics parameters of concrete from uniaxial tests as influenced by specimen length." *Proc. SEM-RILEM Int. Conf. on Fracture of Concrete and Rock*, 31(2), S. P. Shah, and S. E. Swartz, eds., 138–149.

Hoshikuma, J., Kawashima, K., Nagaya, K., and Taylor, A. W. (1997). "Stress-strain model for confined reinforced concrete in bridge piers." *J. Struct. Eng.*, 10.1061/(ASCE)0733-9445(1997)123:5(624), 624–633.

Kent, D. C., and Park, R. (1971). "Flexural members with confined concrete." *J. Struct. Div.*, 97(7), 1969–1990.

Lotfi, H. R., and Shing, P. B. (1991). "An appraisal of smeared crack models for shear wall analysis." *Comput. Struct.*, 41(3), 413–425.

Lotfi, H. R., and Shing, P. B. (1994). "Interface model applied to fracture of masonry structures." *J. Struct. Eng.*, 10.1061/(ASCE)0733-9445(1994)120:1(63), 63–81.

Lourenço, P. B., Milani, G., Tralli, A., and Zucchini, A. (2007). "Analysis of masonry structures: Review of and recent trends in homogenization techniques." *Can. J. Civ. Eng.*, 34(11), 1443–1447.

Lourenço, P. B., and Rots, J. G. (1997). "Multisurface interface model for analysis of masonry structures." *J. Eng. Mech.*, 10.1061/(ASCE)0733-9399(1997)123:7(660), 660–668.

Magenes, G., Kingsley, G., and Calvi, G. M. (1995). "Seismic testing of a full-scale, two storey masonry building: test procedure and measured experimental response." *Rep. 3.0*, CNR-GNDT, Italy.

Pauley, T., and Priestley, M. J. N. (1992). *Seismic design of reinforced concrete and masonry buildings*, Wiley, New York, 106–114.

Priestley, M. J. N., and Elder, D. M. (1983). "Stress-strain curves for unconfined and confined concrete masonry." *J. Am. Concr. Inst.*, 80(3), 192–201.

Rots, J. G. (1997). *Structural masonry: An experimental/numerical basis for practical design rules*, Balkema, Rotterdam, The Netherlands.

Van Der Pluijm, R., and Vermeltfoort, A. T. (1991). "Deformation controlled tension and compression tests in units, mortar and masonry." *Rep. B-91-0561*, TNO-Bouw, Delft, The Netherlands.

Vecchio, F. J. (1990). "Reinforced concrete membrane element formulations." *J. Struct. Eng.*, 10.1061/(ASCE)0733-9445(1990)116:3(730), 730–750.

Vecchio, F. J. (1992). "Finite element modeling of concrete expansion and confinement." *J. Struct. Eng.*, 10.1061/(ASCE)0733-9445(1992)118:9(2390), 2390–2406.

Vecchio, F. J. (2000). "Disturbed stress field model for reinforced concrete: formulation." *J. Struct. Eng.*, 10.1061/(ASCE)0733-9445(2000)126:9(1070), 1070–1077.

Vecchio, F. J. (2001). "Disturbed stress field model for reinforced concrete: implementation." *J. Struct. Eng.*, 10.1061/(ASCE)0733-9445(2001)127:1(12), 12–20.

Vecchio, F. J., and Collins, M. P. (1993). "Compression response of cracked reinforced concrete." *J. Struct. Eng.*, 10.1061/(ASCE)0733-9445(1993)119:12(3590), 3590–3610.

Wong, P. S., and Vecchio, F. J. (2002). "VecTor 2 & formworks user's manual." Dept. of Civil Engineering, Univ. of Toronto, Toronto, ON.

Weaver, W., Jr., and Johnson, P. R. (1984). *Finite elements for structural analysis*, Prentice Hall, Englewood Cliffs, NJ.